RESEARCH PAPER

Optimizing Organic Solar Cells: The Effect of P3HT:PCBM Active Layer and Ca Interference Layer

Brioua Fathi[1,*], Daoudi Chouaib[2]

* *brioua.f@univ-adrar.edu.dz*

[1] Département Génie Électrique, Université Ahmed Draia, route national N°6, Adrar, Algeria
[2] Département de Génie Électrique, Université 20 Août 1955, Skikda, B.P.26 route d'El-Hadaiek Skikda 21000 Skikda, Algeria

Abstract: We have modelled theoretical incident photon-to-current electricity (IPCE) action spectra of poly (3-hexylthiophene) (P3HT) and [6, 6]-Phenyl C61 butyric acid methyl ester active layer bulk-heterojunction. By the two-dimensional optical model of a multilayer system based on the structure of Glass substrate /SiO₂/ITO/PEDOT: PSS/P3HT: PCBM(1:1)/Ca/Al, the optical responses of the device have been computed for different photoactive layer and Ca layer thicknesses to found an optimal structure which allows obtaining the maximum absorption localized in the active layer and high device performance. The electric field intensity, energy dissipation, generation rate, and IPCE have been computed to enhance the device's performance. The finite element method executes the simulation under an incident intensity of 100 mW/cm² of the 1.5 AM illumination. It was found that the optimum structure is achieved by a 180 nm photoactive layer and 5 nm Ca layer thicknesses.

Keywords: Organic solar cells, Optical responses, Optimal structure, Absorption, Generation rate, Modeling.

1. INTRODUCTION

Organic solar cells (OSCs) have attracted considerable attention due to their properties and advantages, such as flexibility, low cost, lightweight, and large-area production [1-3]. The progress in this type of energy knows an increase in the last layer from the small molecular solar cell [4] and bi-layer solar cells [5] to bulk heterojunction (BHJ) polymer, in which the blended composite is a mix of donor and acceptor materials, which is allowed to configure large phase-separated interface area and high the probability of exciton dissociation [4]. Among the BHJ polymers that exhibit an essential efficiency, the P3HT and PCBM donor and the acceptor materials, respectively, up to 3-5% [6]. However, the efficiency is still low compared to other solar cell types, which know rapid efficiency growth and stability similar to perovskite solar cells [7]. Several studies address improving the efficiency of OSCs; Waqas et al. studied [8] two distinct topologies of thin-film OSCs employing various materials. Their main objective is to optimize the thickness of the active layers to achieve optimal sunlight absorption. The results indicate that a thickness of 200 nm effectively covers the visible spectrum, leading to enhanced efficiency. The study emphasizes the substantial absorption of

photons in the active region and demonstrates a 0.97% efficiency advantage for the structure based on fullerene.

Other theoretical approaches have focused on understanding the principle of function of the OSCs to enhance their efficiencies, as our previous study [9], in addition to some important works of D. D. Y. Setsoafia et al. [10], and X. Zhao et al. [11], which are based on applied optical and electrical models. The previous investigations were conducted to optimize the thickness of the blend layer. A direct correlation was discovered between the growth of active layer thicknesses and the improvement in light absorption, as well as a decrease in the strength of the electric field resulting from reduced exciton dissociation and charge collecting [9-11].

Yue Zang et al. [12] study microcavity OSCs incorporating photoactive layers to improve light-harvesting efficiency. They optimize device designs using optical simulations and discover that microcavity OSCs with a ZnO/Ag/ZnO electrode have lower photocurrent than ITO-based devices for layers above 800 nm. Despite this, they suggest a top-illuminated microcavity architecture for narrow bandgap systems with ITO-like photocurrent. Their discoveries help optimize microcavity effects, notably in non-fullerene systems, for highly efficient large-area

Brioua Fathi et al.

flexible OSC devices.

In this paper, an optical model has been proposed to predict the optical responses and IPCE of the device using simple analytical equations. To achieve higher performance of the device, we applied numerical modelling of a structure based on glass substrate/SiO$_2$/a transparent Indium Tin Oxide (ITO)-electrode/Poly(3,4-ethylene dioxythiophene) poly(styrene sulfonate) (PEDOT: PSS)/bulk heterojunction blend of poly(3-hexylthiophene) mixed with [6,6]-Phenyl C61 butyric acid methyl ester (P3HT: PCBM) (1:1) as photo-active material/Calcium (Ca)/ backside contact of aluminum (Al) as shown in Fig. 1. Simulations are performed using the finite element method with COMSOL Multiphysics [13].
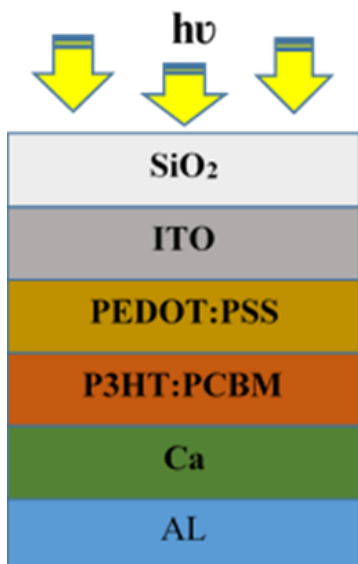
Fig. 1. Schematic diagram of OSC device based on P3HT: PCBM Blend.

2. MODEL

To evaluate the optical responses of the device, the input of the optical simulation is needed as the intensity of incident light for a range of wavelengths, which can be obtained by approximating the Guangyong Li et al. [14] proposed that the irradiation of the standard solar AM1.5 is a blackbody radiator, as mentioned in the flowing equation:

$$I_0(\lambda) = \frac{2\hbar\pi c^2}{\lambda^5} \frac{1}{e^{\hbar c/\lambda k_B T} - 1}$$

(1)

Where (I_0) is the monochromatic light source intensity as a function of the wavelength (λ), (h)

is the Planck constant, (k_B) is the Boltzmann constant, (c) is the velocity of light in vacuum, and (T) is the temperature. In addition to the incoming light propagation excitation, which penetrates the device through the glass substrate/SiO$_2$ side towards the Al electrode by a normal incidence (0 deg) under the form of transmission and reflection simultaneously in the range between 300 to 800 nm wavelengths, all complex refractive index parameters of the device layers must be defined [11].

The Optical indices n (λ) and extinction coefficients k (λ) of the P3HT: PCBM Blend OSCs on function wavelength used in this contribution are given from [14]. As well as to the optical constants of PEDOT: PSS, ITO, Ca, and Al, are obtained from [14-16]. Also, the thicknesses of the device structure are suggested as 1 mm glass substrate/10 nm SiO$_2$/ITO (110 nm)/40 nm of PEDOT: PSS/(x nm) various thicknesses active layer P3HT: PCBM with a ratio of (1:1)/(x nm) various thick of Ca/80 nm a sufficient thick Al back contact.

The optical model used in this study is based on the parameters described in the previous section, which has already been explained in good detail in [9], here it is very briefly described. However, the exciton generation rate per unit volume, G(r), at point r= (x, y), can be precisely determined using the following equation [9]:

$$G(r) = \int_{\lambda_1}^{\lambda_2} \frac{\lambda}{hc} Q(z,\lambda) d\lambda$$

(1)

Where Q(z, λ) is the average of the energy dissipation per unit of time at the position z under wavelength λ.

3. RESULTS AND DISCUSSION

Device performance is dependent on optical responses such as the electric field intensity and optical absorption inside the device. These responses allow us to predict the value of the generation of photo-induced excitons. The optical model, as described in the previous section, simulates this process.

3.1. Electrical Field Intensity

Fig. 2 shows the distribution of the square modulus of the electric field amplitude inside the device on the function of the various thicknesses of the Ca layer under different wavelengths of 400 nm and 500 nm of light.

In the first case of 20 nm Ca thickness and under 400 nm wavelength, the maximum electric field intensity reached is around 25 (a.u) located in P3HT: PCBM layers and then continuously decreases down to Ca layer, finally equal zero in the Al layer due to the optical interference [9] as shown in Fig. 2a.

In the second case for 5 nm Ca thickness, an increase of 25% in the value of the electric field intensity reaches around 30 (a.u), with localization at the position between PEDOT: PSS and P3HT: PCBM in the device as shown in Fig. 2b. Finally, the same observation has been obtained in the case of 500 nm wavelength as shown in Fig. 2c and Fig. 2d.
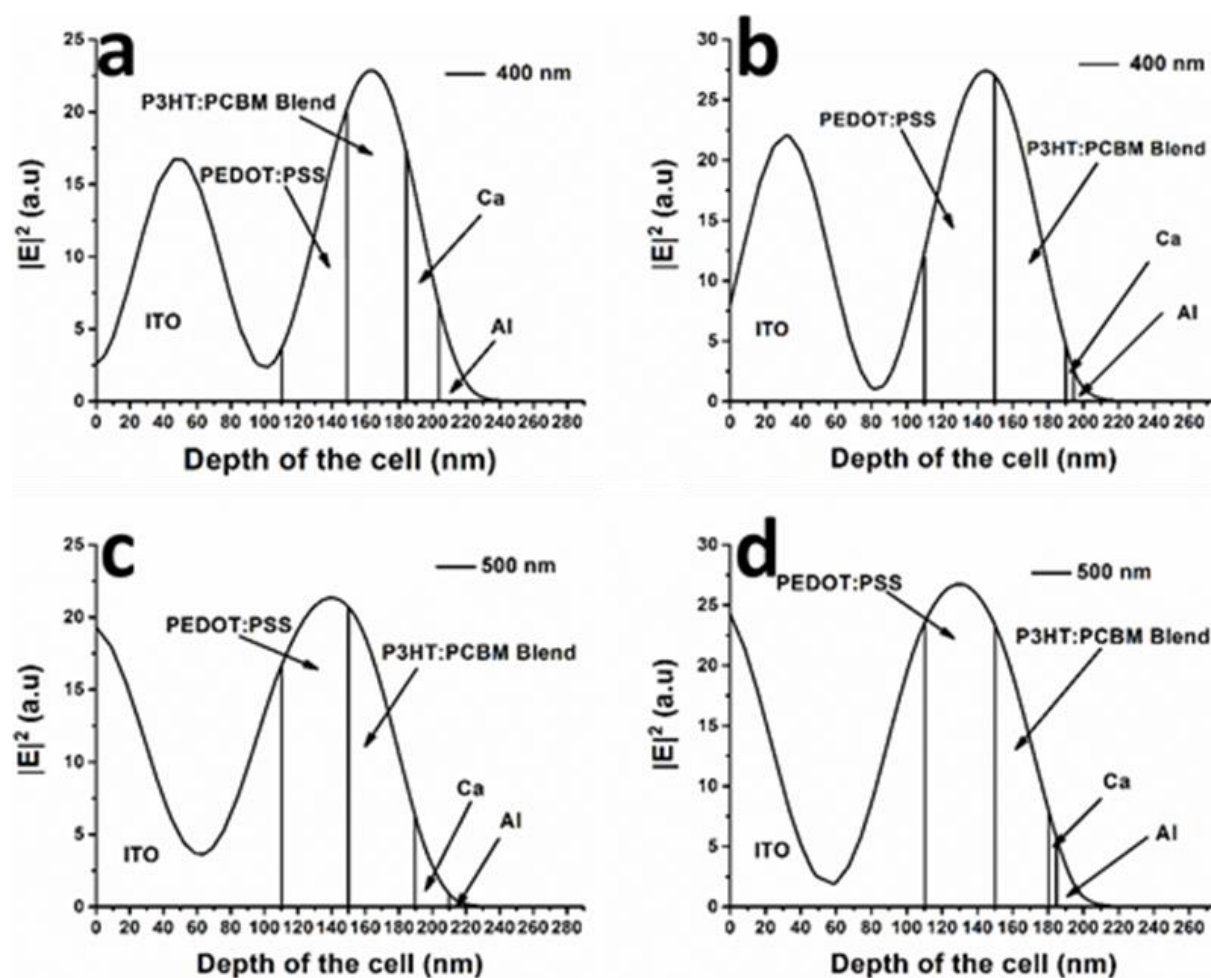
3.2. Energy Dissipated

As shown in Fig. 3a and Fig. 3b, the profiles of the energy dissipated in the device with 5 nm Ca thickness were calculated under 400 nm and 500 nm wavelengths in the solar spectrum, which are calculated from the equations mentioned in the optical model of D. D. Y. Setsoafia et al. [10].

3.3. Generation Rate

Fig. 4, shows the evolution of the total generation rate profiles versus different active layer thicknesses (55 and 180 nm), with a structure solar cell based on the 5 nm Ca thickness layer under 650 nm wavelength. Equation 2 gives the generation rate profile.

We can show that total generation rate profiles take values differently depending on the thicknesses of the active layer and with an oscillator behavior. For example, a value of 1.27 e^{28} (cm^{-3} x s^{-1}) has been obtained in the case of 55 nm active layer thickness, then increases up to 1.5 e^{28} (cm^{-3} x s^{-1}) for 180 nm active layer thickness due to the interference effects, this is in agreement with the results reported by several researches [9, 17].

Fig. 2. Distribution of $|E|^2$ inside the device, as a function of different Ca layer thicknesses (20 nm and 5 nm) in 400 nm (a, b) and 500 nm (c, d) wavelengths.

3

Fig. 3. Distribution of the dissipated energy versus the thicknesses of the solar cell with 5 nm Ca.

Fig. 4. Profiles of generation rate for various 55 and 180 nm blend thicknesses and 5 nm thick Ca under 650 nm wavelength.

3.4. IPCE

The IPCE represents the spectral response and generation rate (%) of conversion of the light intensity to electron-hole pair and was calculated to evaluate the optical response of the device performance on function the wavelengths for two standard structure devices (55 and 180 nm) of P3HT: PCBM thicknesses with 5 nm Ca thickness as shown in Fig. 5. Similar behavior has been obtained for two cases, with a maximum response reaching 1.05 at 550 nm wavelength. However, a significantly higher IPCE response of approximately 16% has been achieved for the 180 nm case compared to the 55 nm case. This discrepancy in IPCE values can be attributed to various factors, including the highest electric field intensity, generation rate, losses due to high reflection and low absorption responses, and the influence of charge recombination [18].
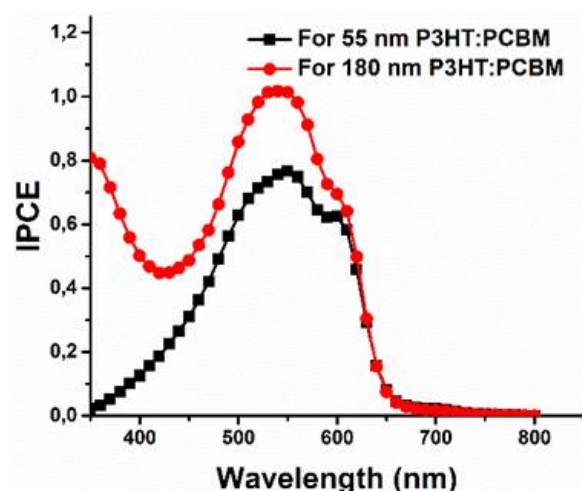

Fig. 5. IPCE values of P3HT: PCBM blend various thicknesses with 5 nm Ca thickness at wavelengths

Additionally, it can be demonstrated through IPCE spectra that within the lower wavelength

4

range of 350-500 nm, distinct differences in IPCE responses have been observed between the two cases, corresponding to the high and low absorption spectra. This is followed by a sharp decrease at higher wavelengths, specifically in the 600 to 800 nm range, which can be attributed to the high reflection, as previously mentioned in other studies [9].

4. CONCLUSIONS

In summary, the effects of each P3HT: PCBM and Ca film thickness on the performance of the OSCs were investigated. Hence, the optical modelling was applied to place the maximum electric field at the interface of the P3HT: PCBM active layer. In addition, it is found that the optical interference effect significantly influences performance. The probability that all photons absorbed within the P3HT: PCBM active layer may contribute to the charge generation is highest with a 5 nm Ca structure due to the high dissipated energy in the P3HT: PCBM blend, which is related to the high values of electric fields intensity under the effect of the optical interference. The generation rate for 5 nm Ca and various active layer thicknesses have been computed. The high value of IPCE is 1.05 for the 5 nm Ca thickness and 180 nm P3HT: PCBM thickness at 550 nm wavelength, which allows us to predict it is the optimal structure for the device's high performance.

REFERENCES

[1]. Tarikhum, H, Abdullah, A. B., Almyahi, F. and Mahdi, M., "Effect of Poly(3-Hexylthiophene):Mixed Fullerene Indene-C60 Multi-Adducts Ratios on the Performance of Organic Solar Cells." IJMSE., 2023, 20(2), 86-99.

[2]. Zhao, F., Zuo, L., Li, Y., Zhan, L., Li, S., Li, X., Xia, R., Yip, H., and Chen, H., "High-Performance Upscaled Indium Tin Oxide–Free Organic Solar Cells with Visual Esthetics and Flexibility." Solar RRL., 2021, 5(9), 2100339.

[3]. Sun, Y., Liu, T., Kan, Y., Gao, K., Tang, B., and Li, Y., "Flexible Organic Solar Cells: Progress and Challenges." Small Sci, 2021, 1(5), 2100001.

[4]. Nelson, J.,. "Organic photovoltaic films." Curr. Opin. in Sol. Sta. and Mater. Sci., 2002, 6(1), 87–95.

[5]. Rugma, S., Devu, B., and Sreekala, C.O., "Effect of Alkyl Substitution to the Active Layer Material for Improved Efficiency in Bilayer Organic Solar Cell." IOP Conf. Ser.: Mater. Sci. Eng., 2022, 1225(1), 012022.

[6]. Shaban, M., Benghanem, M., Almohammedi, A., and Rabia, M., "Optimization of the Active Layer P3HT: PCBM for Organic Solar Cell." Coat., 2021, 11(7), 863.

[7]. Stranks, S.D., Eperon, G.E., Grancini, G., Menelaou, C., Alcocer, M.J.P., Leijtens, T., Herz, L.M., Petrozza, A., and Snaith, H.J., "Electron-Hole Diffusion Lengths Exceeding 1 Micrometer in an Organometal Trihalide Perovskite Absorber." Sci., 2013, 342(6156), 341–344.

[8]. Farooq, W. A Alzahrani, A., and Ghoneim, S.S.M., "Computational optimization and optical analysis of thin‑film organic solar cells for high efficiency." J. of Comput. Electron., 2023, 22, 867–873.

[9]. Brioua, F., Remram, M., Nechache, R., and Bourouina, H., "Electrical and optical modeling of poly(3-hexylthiophene):[6,6]-phenyl-C61 butyric acid methyl ester P3HT–PCBM bulk heterojunction solar cells." Appl. Phys. A, 2017, 123(11), 704.

[10]. Setsoafia, D.D.Y., Ram, K.S., Rad, H.M., Ompong, D., Elumalai, N.K., Singh, J., "Optimizing Device Structure of PTB7-Th: PNDI-T10 Bulk Heterojunction Polymer Solar Cells by Enhancing Optical Absorption." Ener., 2022, 15, 711.

[11]. Zhao, X., Gu, H., Chen, L., Liu, S., "Optical Model and Optimization for Coherent-Incoherent Hybrid Organic Solar Cells with Nanostructures." Nano., 2021, 11, 3187.

[12]. Zang, Y., Liu, Y., Chen, L., Xu, R., Wang, Y., Yan, W., "Optical modeling of microcavity strategy for highly efficient ITO-free organic solar cells with varied photoactive layers." Opt. Mater., 2022, 132, 112772.

[13]. Moës, N., Dolbow, J., and Belytschko, T., "A finite element method for crack growth without remeshing." Int. J. for Numer. Methods in Eng, 1999, 46(1), 131–150.

[14]. Li, G., Liu, L., Wei, F., Xia, S., and Qian,

X., "Recent Progress in Modeling, Simulation, and Optimization of Polymer Solar Cells." IEEE J. Photovolt., 2012, 2(3), 320–340.

[15]. Mathewson, A.G., and Myers, H.P., "Absolute Values of the Optical Constants of Some Pure Metals." Phys. Scr., 1971, 4(6), 291.

[16]. Rahmani, R., Karimi, H., Ranjbari, L., Emadi, M., Seyedmahmoudian, M., Shafiabady, A. and Ismail, R., "Structure and Thickness Optimization of Active Layer in Nanoscale Organic Solar Cells." Plasm., 2015, 10, 495–502.

[17]. Chowdhury, M.M., and Alam, M.K., "An analytical model for bulk heterojunction organic solar cells using a new empirical expression of space dependent photocarrier generation." Sol. Ener., 2016, 126, 64–72.

[18]. Park, S.H., Roy, A., Beaupré, S., Cho, S., Coates, N., Moon, J.S., Moses, D., Leclerc, M., Lee, K., and Heeger, A.J., "Bulk heterojunction solar cells with internal quantum efficiency approaching 100%." Nat. Photon. 2009, 3(5), 297-302.